Agricultural and Forest Meteorology 237–238 (2017) 60–70

Contents lists available at ScienceDirect

Agricultural and Forest Meteorology

journal homepage: www.elsevier.com/locate/agrformet

Examining the short-term impacts of diverse management practices on plant phenology and carbon fluxes of Old World bluestems pasture

Yuting Zhou[a], Xiangming Xiao[a,b,*], Pradeep Wagle[c], Rajen Bajgain[a], Hayden Mahan[d], Jeffrey B. Basara[d,e], Jinwei Dong[a], Yuanwei Qin[a], Geli Zhang[a], Yiqi Luo[a], Prasanna H. Gowda[c], James P.S. Neel[c], Patrick J. Starks[c], Jean L. Steiner[c]

[a] Department of Microbiology and Plant Biology, Center for Spatial Analysis, University of Oklahoma, Norman, OK 73019, USA
[b] Ministry of Education Key Laboratory of Biodiversity Science and Ecological Engineering, Institute of Biodiversity Science, Fudan University, Shanghai, 200433, China
[c] USDA–ARS Grazinglands Research Laboratory, El Reno, OK 73036, USA
[d] School of Meteorology, University of Oklahoma, Norman, OK 73019, USA
[e] Oklahoma Climate Survey, Norman, OK 73019, USA

ARTICLE INFO

Article history:
Received 30 September 2016
Received in revised form 9 January 2017
Accepted 29 January 2017
Available online 10 February 2017

Keywords:
PhenoCam images
Green chromatic coordinate (GCC)
Gross primary production (GPP)
Plant phenology
Vegetation photosynthesis model (VPM)
Eddy covariance (EC)

ABSTRACT

Burning, grazing, and baling (hay harvesting) are common management practices in grassland. To develop and adopt sustainable management practices, it is essential to better understand and quantify the impacts of management practices on plant phenology and carbon fluxes. In this study, we combined multiple data sources, including *in-situ* PhenoCam digital images, eddy covariance data, and satellite data (Landsat and Moderate Resolution Imaging Spectroradiometer (MODIS)) to examine the impacts of burning, baling, and grazing on canopy dynamics, plant phenology, and carbon fluxes in a pasture in El Reno, Oklahoma in 2014. Landsat images were used to assess the baling area and the trajectory of vegetation recovery. MODIS vegetation indices (VIs) were used in the Vegetation Photosynthesis Model (VPM) to estimate gross primary production (GPP_{VPM}) at a MODIS pixel for the flux tower (baled) site. For comparison between baled and unbaled conditions, we used MODIS VIs for a neighbor MODIS pixel (unbaled) and ran VPM. Daily PhenoCam images and green chromatic coordinate (GCC) tracked canopy dynamics and plant phenology well. The grassland greened up immediately after burning in April. GCC values showed two peaks with the similar magnitude because of quick recovery of grassland after baling. Satellite-derived VIs and GPP_{VPM} showed that the pasture recovered in one month after baling. The GPP_{VPM} matched well ($R^2 = 0.89$) with the eddy covariance-derived GPP (GPP_{EC}). Grazing in the late growing season did not influence plant phenology (VIs and GCC) and carbon uptake (GPP) as plants were in the late growing stage. Neither did it affect GPP differently in those two conditions because of even grazing intensity. The reduction in GPP after baling was compensated by higher GPP after large rain events in late July and early September, causing little seasonal differences in GPP (-0.002 g C m^{-2} day^{-1}) between the baled and unbaled conditions. Interactions of different management practices with climate make it complicated to understand the impacts of different management practices on carbon dynamics and plant phenology. Thus, it is necessary to further investigate the responses of pastures to different management practices under different climate regimes at multiple temporal and spatial scales.

1. Introduction

Grassland (both native prairie and planted/introduced pasture) is a major forage source for millions of beef cattle in the Great Plains of the United States. Management practices in pasture are diverse (e.g., burning, grazing, baling, fertilizing), complex (e.g., mixture of management practices such as grazing and baling, different duration and timing), and can vary over space and time. Prescribed burning is a recommended management practice to

* Corresponding author at: Department of Microbiology and Plant Biology, Center for Spatial Analysis, University of Oklahoma, 101 David L. Boren Blvd Norman, OK 73019, USA.
E-mail address: xiangming.xiao@ou.edu (X. Xiao).

http://dx.doi.org/10.1016/j.agrformet.2017.01.018
0168-1923/

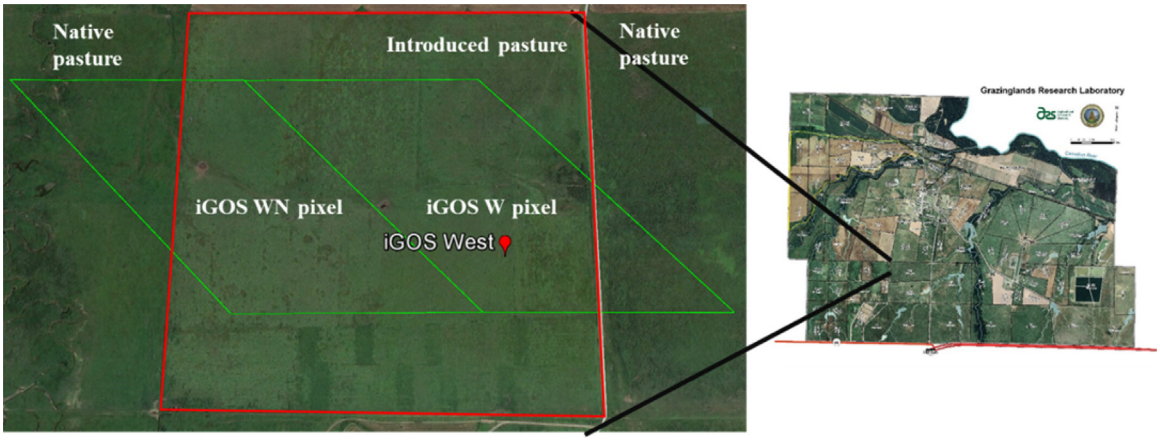

Fig. 1. Location of flux tower site and overlapping with MODIS pixels. Location of the flux tower site is marked as red point and labeled. Red rectangle is the boundary of the study field. Green diamonds are boundaries of MODIS pixels. (For interpretation of the references to colour in this figure legend, the reader is referred to the web version of this article.)

recycle plant nutrients, remove senesced vegetation, and to control weeds and inhibit woody species encroachment (Brockway et al., 2002; Reinhart et al., 2016; Twidwell et al., 2013; Valkó et al., 2014). Grazing and baling remove aboveground biomass and reduce canopy coverage and vegetation photosynthesis. The effects of grazing on carbon fluxes (e.g., gross primary production, GPP) vary under different ecological conditions and grazing intensity (Rogiers et al., 2005). Field experiments that mechanically clip vegetation to mimic hay or biofuel feedstock harvest, showed that grassland ecosystems may not be a sink of carbon depending on the amount of biomass removal (Luo et al., 2009; Niu et al., 2013; Wagle and Kakani 2014). These management practices can have multiple impacts on vegetation canopy, phenology, and carbon dynamics (Campioli et al., 2015; Wilson et al., 2013). Thus, it is a challenging task to track those management practices and assess their impacts on pasture as well as beef cattle production.

A number of tools are available to study the impacts of management practices on vegetation phenology and carbon fluxes of grasslands, including *in-situ* digital cameras (PhenoCam), eddy covariance (EC) measurements, and satellite remote sensing. PhenoCam takes multiple digital photography in a day and provides "near surface" observations of plant phenology with high temporal resolution (Migliavacca et al., 2011; Richardson et al., 2009). Satellite remote sensing acquires consistent and periodic observations of the land surface to track vegetation phenology (Zhang et al., 2003). Vegetation indices (VIs) derived from satellite images are also used in production efficiency models to estimate gross and net primary production of vegetation (Potter et al., 1993; Running et al., 2004; Sims et al., 2008; Wu et al., 2010; Xiao et al., 2004a; Xiao et al., 2004b; Yuan et al., 2007). Because of the higher temporal resolution (8-day), the Moderate Resolution Imaging Spectroradiometer (MODIS) is used more often in GPP modeling than Landsat which has a higher spatial resolution (30 m) but lower temporal resolution (16-day). EC observations reflect effects of land use and management on the exchange of carbon dioxide, water vapor, and energy fluxes (Chi et al., 2016; Fischer et al., 2012; Owensby et al., 2006; Suyker et al., 2003). As the footprint of eddy flux tower is often comparable with the spatial resolution of the MODIS surface reflectance products, EC-derived GPP (GPP_{EC}) are widely used to evaluate modeled GPP using MODIS data (Dong et al., 2015; Jin et al., 2013; Sims et al., 2008; Wagle et al., 2014; Wu et al., 2010; Yuan et al., 2007).

Although field experiments help to examine the effects of management practices on carbon dynamics (Luo et al., 2009; Niu et al., 2013; Wagle and Kakani 2014), the influence of management practices on canopy scale carbon dynamics is not well understood, necessitating the integration of EC and remote sensing observations to study the effects of grazing, baling, or other management practices on canopy and carbon dynamics. Ideally, paired towers are needed in both the control and manipulated (e.g., unbaled and baled) area for the comparison. However, the high construction cost and logistical requirements of EC systems prohibit the utilization of paired towers in most cases (Chi et al., 2016; Fischer et al., 2012). Alternatively, modeling approaches can be used. Remote sensing-based production efficiency models estimate GPP as the product of the absorbed photosynthetically active radiation (APAR) and light use efficiency (LUE, ϵg) (Potter et al., 1993; Running et al., 2004; Xiao et al., 2004a; Xiao et al., 2004b; Yuan et al., 2007). Most of these models use VIs and meteorological parameters as inputs. In the case of a single eddy flux tower site with disturbances or management practices, VIs of the nearby undisturbed area of similar vegetation cover, can be combined with the meteorological parameters of the flux tower site to simulate GPP for the undisturbed condition. By comparing the two scenarios (e.g., baled and unbaled), we can show the effects of management practices or disturbances on GPP.

The objective of this study is to examine the impacts of burning, baling, and grazing on canopy and carbon fluxes in a pasture through integrating PhenoCam images, satellite remote sensing, and eddy covariance data. In addition, the impacts of management practices (e.g., baling and grazing) on GPP were investigated using the satellite-based vegetation photosynthesis model (VPM) for disturbed and undisturbed conditions. This case study, using multiple observation techniques to detect the impacts of diverse management practices, can serve as an example of utilizing different data sources to better understand the impacts of management practices on vegetation phenology and carbon fluxes.

2. Materials and methods

2.1. Study site description

The study site (Fig. 1) is located at the United States Department of Agriculture—Agricultural Research Service (USDA-ARS) Grazinglands Research Laboratory (GRL) in El Reno, Oklahoma (35.54679°N, 98.04529°W, 435 m above sea level). The field (red rectangle in Fig. 1) is an introduced warm-season, pasture which was planted with old world bluestem (*Bothriochloa caucasica* C. E. Hubb.) (Samuel and Forbes 1998). The pasture's soil is classified as Norge silt loam (Fine-silty, mixed, active, thermic Udic Paleustolls) (Staff 1999) with a depth greater than 1 m and high water holding capacity (Fischer et al., 2012).

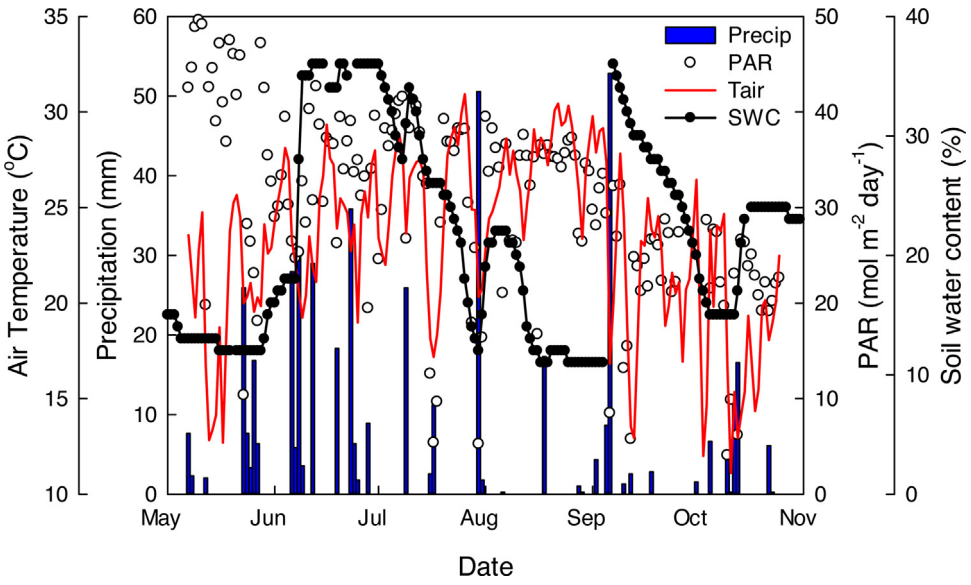

Fig. 2. Seasonal dynamics of photosynthetically active radiation (PAR), precipitation (Precip), air temperature (Tair), and soil water content (SWC) at 25 cm observed at the flux tower site/nearby Mesonet site. Each data point represents daily average.

Several management activities (e.g., burning, fertilizer and herbicide applications, baling for hay, and cattle grazing) were implemented at the site in the same year (2014). The field was burned on April 9th (DOY 99) and sprayed on May 1st with herbicide (2.35 l/ha of GRAZON) and followed immediately by fertilizer (44.8 kg N/ha 46-0-0) application. In late July, part of the eastern half of the field close to eddy flux tower was cut for hay and baled on July 23rd (DOY 204, the first baling). The remaining part of the eastern half was cut for hay in early August and baled on August 15th (DOY 227, the second baling). Twenty five cows with an average weight of 520 kg continuously grazed the entire field from September 25th (DOY 268) until end of the calendar year.

2.2. Eddy flux tower site and EC data processing

The EC system was deployed at the beginning of May 2014 to measure fluxes of CO_2 and H_2O using a LI–7500 A (LI-COR Biosciences Inc., NE, USA) and CSAT3 sonic anemometer (Campbell Scientific Inc., UT, USA). PhenoCam (StarDot Technologies, CA, USA) images, and other meteorological variables such as surface energy balance components, air temperature, relative humidity, soil temperature, soil water content at 25 cm (SWC), and solar radiation were also included as part of an integrated Grassland Observation System in the west of GRL (iGOSW). The Oklahoma Mesonet El Reno site is 800 m to the east of iGOS W which provides quality-controlled measurements of meteorological and land-surface variables such as precipitation, temperature, and soil moisture at intervals spanning 5–30 min depending on the variables (McPherson et al., 2007) (http://www.Mesonet.org/). Precipitation, photosynthetically active radiation (PAR), air temperature, and SWC at 25 cm are presented in Fig. 2.

The raw 10 Hz EC data were processed using EddyPro software version 5.1.1 (LI-COR Biosciences Inc., NE, USA) to produce 30-min fluxes of CO_2, H_2O, and energy. The EddyPro output results were further screened based on quality assurance/quality control (QA/QC) flags [i.e., fluxes with quality flags of '2 (bad quality)' were rejected]. In addition, fluxes beyond the reliable range of fluxes [i.e., net ecosystem CO_2 exchange, NEE: beyond $\pm 50\ \mu mol\ m^{-2}\ s^{-1}$ (Zeeman et al., 2010)] were also excluded. The EddyPro also provides flux footprint estimations which can show the contribution of flux measurements from different directions and distances for different periods (before and after baling).

Gaps in the flux data were filled using a moving lookup table approach which considers both the covariance of fluxes with meteorological variables and temporal auto-correlation of fluxes (Reichstein et al., 2005). The NEE was partitioned into GPP and ecosystem respiration (ER) based on the temperature sensitivity of ER (Lloyd and Taylor 1994). Both gap filling and partitioning were conducted using the online R package "REddyProc" (https://www.bgc-jena.mpg.de/bgi/index.php/Services/REddyProcWebRPackage), developed at the Max Planck Institute for Biogeochemistry, Jena, Germany (Moffat et al., 2007; Reichstein et al., 2005). Daily sums of NEE, ER, and GPP were presented to show the carbon dynamics for the growing season in 2014 (May-October).

2.3. PhenoCam images and greenness index

Canopy images were collected with a StarDot NetCam SC camera installed in a weatherproof enclosure at a height of 3.0 m above the ground. The camera was pointed south and set at an angle of about 20° below horizontal. The camera provides regular RGB images for the same scene as the camera position was fixed. Various greenness indices can be derived from the PhenoCam images to detect the plant phenology (Richardson et al., 2007). For this study, the green chromatic coordinate (GCC) value was used to indicate the vegetation status for one specific "Region of Interest" (ROI) located in the baling affected area (black rectangle showed in Fig. 3e) using the following equation (Eq. (1)):

$$GCC = \frac{G_{DN}}{R_{DN} + G_{DN} + B_{DN}} \quad (1)$$

where R_{DN}, G_{DN}, B_{DN} are RGB digital numbers (DN). The time series of GCC values were calculated using the PhenoCam toolkit from PhenoCam network (https://phenocam.sr.unh.edu/webcam/tools/).

2.4. MODIS images and VIs

The 8-day composite MODIS surface reflectance product (MOD09A1) (Vermote and Vermeulen 1999) was used to investigate the seasonal dynamics of the VIs for the flux tower located

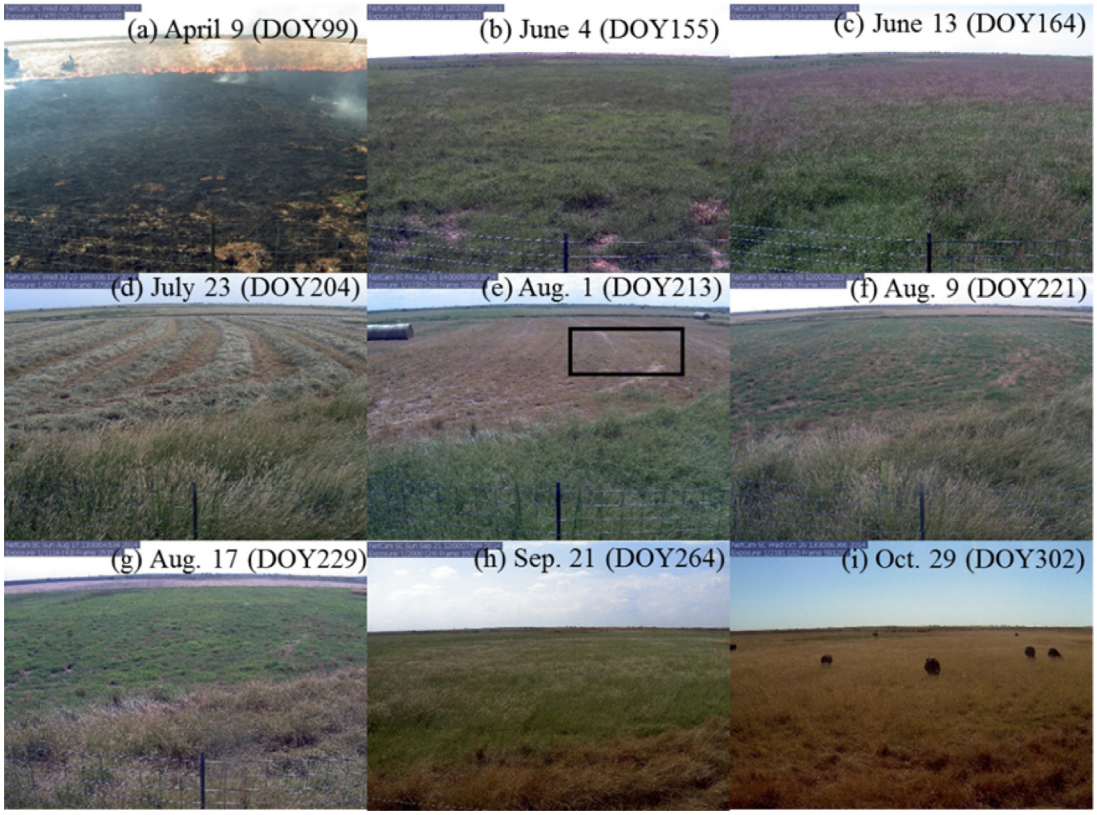

Fig. 3. PhenoCam images showing management practices and phenology of grassland. The black rectangle in panel e shows the region of interest (ROI) used to calculated GCC values.

pixel (iGOS W) and for its neighbor pixel (iGOS WN) (Fig. 1). The majority of both iGOS W and iGOS WN MODIS pixels are old world bluestem pasture. Both pixels were burned and received applications of fertilizer and herbicide. The first baling only affected iGOS W and the second baling did not affect both pixels which was to the south of the iGOS W pixel. MOD09A1 has reflectance values of the seven spectral bands: blue (459–479 nm), green (545–565 nm), red (620–670 nm), two near infrared (NIR_1: 841–876 nm; NIR_2: 1230–1250 nm), and two shortwave infrared ($SWIR_1$: 1628–1652 nm, $SWIR_2$: 2105–2155 nm) at a 500-m spatial resolution. It also includes quality control flags for consideration of various image artifacts (e.g., clouds and cloud shadow). All data that did not pass the quality control were excluded in further analysis based on the following criteria: cloud state flag indicates cloudy or mixed, or cloud shadow existence, or aerosol quantity flag shows high, or cirrus detected flag is average or high.

Normalized Difference Vegetation Index (NDVI), Enhanced Vegetation Index (EVI), and Land Surface Water Index (LSWI) were calculated from MOD09A1 using surface reflectance (ρ) from blue ($\rho blue$), red (ρred), NIR_1 (ρnir, 841–876 nm), and $SWIR_1$ ($\rho swir$, 1628–1652 nm) bands (Eqs. (2)–(4)). The coefficients C1, C2, and L are 6.0, 7.5, and 1.0, respectively, and G is a gain factor set to 2.5 in EVI calculation (Huete 2002). EVI and LSWI were also used in VPM to simulate GPP. Bad observations of EVI and LSWI values were linearly interpolated using good, nearby observations.

$$NDVI = \frac{\rho_{nir} - \rho_{red}}{\rho_{nir} + \rho_{red}} \quad (2)$$

$$EVI = G \times \frac{\rho_{nir} - \rho_{red}}{\rho_{nir} + C1 \times \rho_{red} - C2 \times \rho_{blue} + L} \quad (3)$$

$$LSWI = \frac{\rho_{nir} - \rho_{swir}}{\rho_{nir} + \rho_{swir}} \quad (4)$$

2.5. Landsat images and VIs

Landsat has higher spatial resolution than MODIS (30 m vs. ~500 m). The baled area was smaller than one MODIS pixel which could introduce error if the baling areas are not examined using higher spatial resolution images. Landsat surface reflectance product (Landsat 7 ETM+ and Landsat 8) covering the study area were downloaded from the USGS EarthExplorer (http://earthexplorer.usgs.gov/) and the images for the study area were extracted. Landsat 8 does not have the same data gap problem as Landsat 7 ETM+ and keeps the same spatial resolution (30 m) (Roy et al., 2014). Fortunately, our study area is located in the center of the image tiles and was not affected by the gaps in Landsat 7 data. Thus, both Landsat 7 ETM+ and Landsat 8 images were included in the analysis. The data quality control approach is similar to use of Landsat imagery in a previous study to exclude the effect of clouds and cirrus observations (Zhou et al., 2016). Shortwave infrared (SWIR-2), near infrared (NIR), and red bands were used to construct false color composite images for use in reducing atmospheric effects and highlight vegetation. EVI and LSWI values for iGOS W and iGOS WN were calculated using Landsat pixels in the corresponding MODIS pixels. The EVI and LSWI differences between iGOS W and iGOS WN derived from MODIS and Landsat for the same period were used to investigate the comparability of these two satellite observations.

2.6. Vegetation photosynthesis model

The Vegetation Photosynthesis Model (VPM) (Xiao et al., 2004a; Xiao et al., 2004b) estimates GPP as the product of light use efficiency (ϵ_g) and absorbed photosynthetically active radiation (APAR) by chlorophyll,

$$GPP_{VPM} = \varepsilon_g \times APAR_{chl} \quad (5)$$

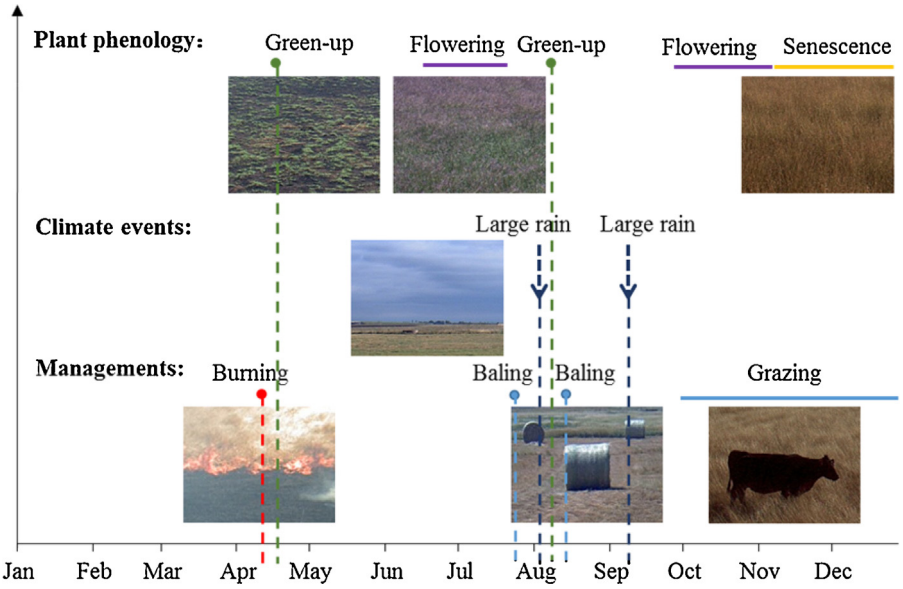

Fig. 4. Management practices, climate events, and plant phenology in the field. The plant phenology was delineated through interpreting individual time series PhenoCam images.

$$APAR_{chl} = fPAR_{chl} \times PAR \quad (6)$$

where $fPAR_{chl}$ is the fraction of PAR absorbed by chlorophyll which is estimated as a linear function of EVI where the coefficient a is set to be 1.0 (Xiao et al., 2004a).

$$fPAR_{chl} = a \times EVI \quad (7)$$

The ϵ_g is derived by down-regulating the theoretical maximum light use efficiency (ϵ_0) with scalars of temperature (T_{scalar}) and water (W_{scalar}) stresses.

$$\varepsilon_g = \varepsilon_0 \times T_{scalar} \times W_{scalar} \quad (8)$$

More information about the T_{scalar} and W_{scalar} can be found in previous studies (Wagle et al., 2014; Xiao et al., 2004a; Xiao et al., 2004b).

The site-specific ϵ_0 is usually determined using a rectangular hyperbola light-response function (NEE-PAR relationship) at 30-min intervals during peak growing season (Falge et al., 2001). For this study the ϵ_0 is set to be 0.062 mol CO_2 mol^{-1} PPFD (PPFD represents photosynthetic photon flux density) which was used for nearby tallgrass prairie sites in a previous study (Wagle et al., 2014).

We first ran VPM for flux tower located MODIS pixel to determine GPP for iGOS W (GPP_{VPM_W}). Then we used the same PAR, air temperature and VIs of the nearby MODIS pixel to simulate GPP for iGOS WN (GPP_{VPM_WN}). This substitution should introduce minimal error as PAR and air temperature do not vary significantly at the scale of one MODIS pixel (~500 m) in flat terrain. GPP_{VPM_W} was compared with the EC derived GPP (GPP_{EC}) to evaluate the performance of VPM. The dynamics of GPP_{VPM_W} and GPP_{VPM_WN} were plotted to visually examine the course of grassland recovery after disturbance due to different management practices (e.g., baling). The differences in GPP sums between the two MODIS pixels indicate the cumulative impacts of disturbances/management practices.

2.7. Statistical analysis

A simple linear regression model was used to investigate the relationship between GPP_{EC} and EVI (one of the major inputs in VPM). GPP_{EC} and GPP_{VPM_W} values were compared to assess the validity of the model. The coefficient of determination (r^2) was used to evaluate the model agreement in both statistical analyses. To show the impacts of different management practices, we tabulated GPP for iGOS W and iGOS WN for different periods.

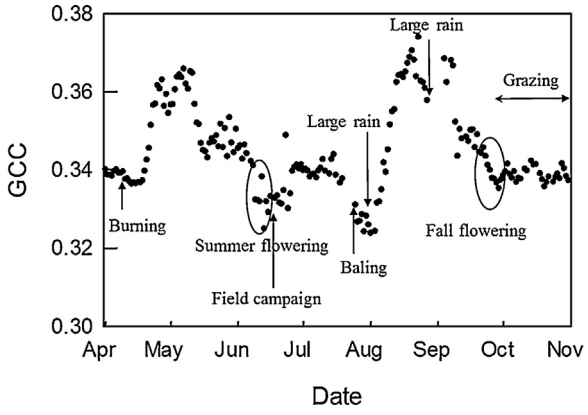

Fig. 5. Daily green chromatic coordinate (GCC) values from PhenoCam images.

3. Results

3.1. Canopy dynamics and plant phenology in response to management practices as observed by PhenoCam, Landsat, and MODIS images

3.1.1. Canopy dynamics and GCC values in response to management practices as observed by PhenoCam images

The real-time images from PhenoCam showed different management practices (burning, baling, and grazing) and phenology of the grassland (Fig. 3) occurred within its field of view. The quick recovery of grasses after baling was also observed in the time-series of PhenoCam images (Fig. 3d and f). The chronology of management practices (the time and period), climate events (rain), and plant phenology is shown in Fig. 4. The GCC values derived from PhenoCam images showed the daily growth dynamics of the vegetation (Fig. 5). The green-up, peak growing season, and senescence stages were clearly reflected by GCC values. While the range of GCC values was small (0.32-0.38), the GCC values showed two peaks at early

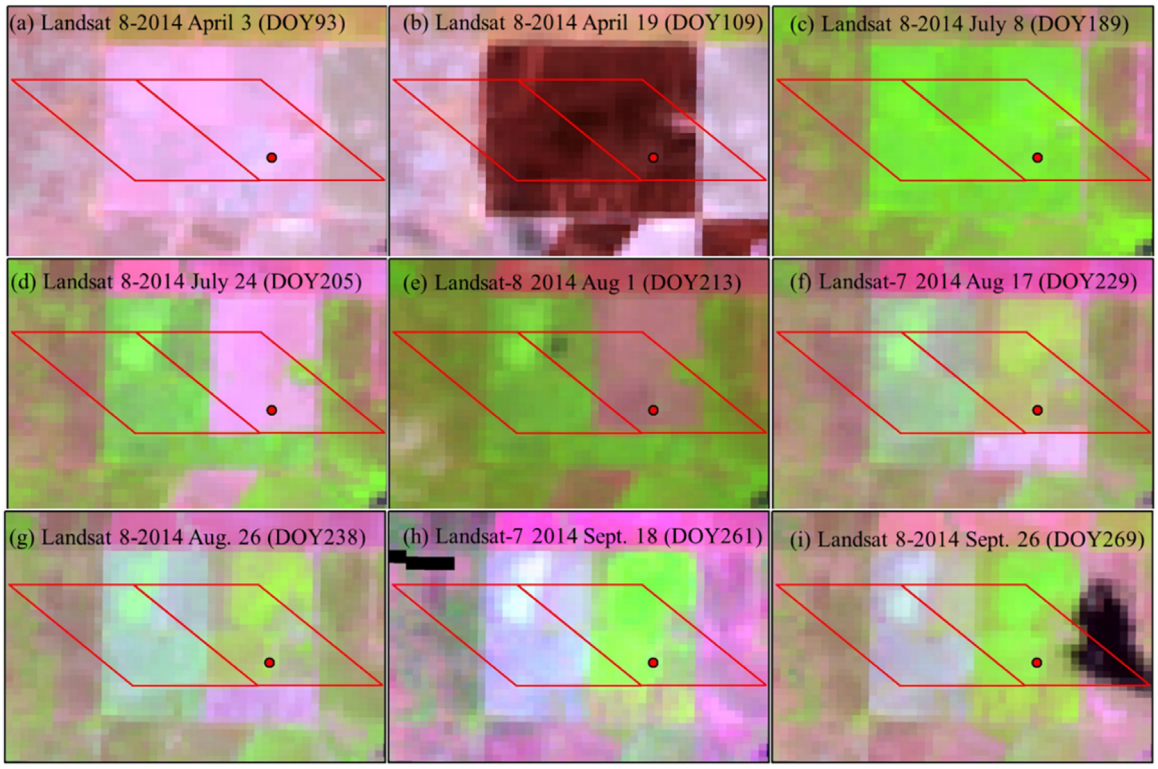

Fig. 6. Landsat images of the study area in different periods. Location of flux tower site and boundaries of MODIS pixels are also shown.

May and mid-August with the magnitude of 0.37-0.38, whereas GCC values during senescence were around 0.34. As expected, the GCC values decreased after baling. However, grazing in the late growing season (September 25th – end of the year) did not affect GCC values.

3.1.2. *Canopy dynamics and plant phenology in response to management practices as observed by landsat images*

The time-series images from Landsat 8 and Landsat 7 ETM+ clearly showed the areas affected by burning and the two baling events (Fig. 6b, d, and f). The Landsat images showed some heterogeneity within the corresponding MODIS pixels. For example, the first baling mostly affected the center of the MODIS pixel for iGOS W (around 67% of the pixel affected) (Fig. 6d). The second baling affected only the area to the south of the MODIS pixel for iGOS W (Fig. 6f). From these images, we can see that the vegetation phenology of the field was quite different than areas outside since the study site is covered by introduced pasture with better vegetation growth than the native pasture. The introduced pasture was much greener than the native pasture in July (Fig. 6c and d) before baling. The area affected by the first baling recovered quickly after one month after cutting (Fig. 6d and f), which was also reflected by high GCC values in mid-August (Fig. 5). The second baling affected area also recovered after about one month (Fig. 6f and i). The introduced pasture (inside field) entered senescence stage much later than the native grassland (outside field) (Fig. 6h and i).

3.1.3. *Plant phenology in response to management practices at iGOS W and iGOS WN as observed by MODIS images*

Dynamics of NDVI, EVI, and LSWI derived from MODIS images for iGOS W and iGOS WN were synchronous from January to early June and from early October to December (Fig. 7). The grassland greened up immediately after burning in April and entered senescence stage at the end of October. LSWI had the most significant drop among three VIs after burning because of SWIR band embedded (Eq. (4)). The lower VIs in mid-June in iGOS WN occurred because of disturbance associated with more frequent sample collection during an intensive field research campaign (Steiner 2014) that was more focused in the western part of the field, where most of MODIS pixel for iGOS WN was located (Fig. 1). The intensive field research campaign investigated multiple aspects of the soil (soil water content and soil greenhouse gas emission) and plant systems (canopy reflectance, leaf area index, canopy height, and aboveground biomass) through sampling soil and plants. VIs values at both MODIS pixels became very similar again at around mid-July. VIs diverged after the first baling in iGOS W on July 23rd. After two big large rain events, VIs of both pixels increased, but VIs at iGOS W increased more. Grazing in the late growing season did not cause

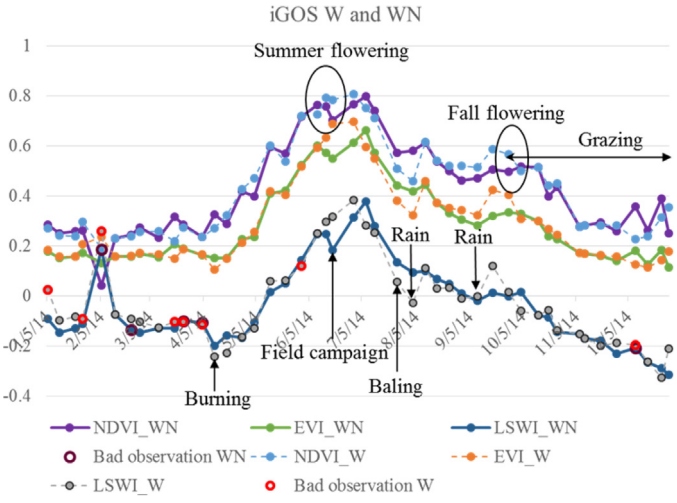

Fig. 7. MODIS vegetation indices (VIs) for the flux tower located pixel (iGOS W) and its neighbor pixel (iGOS WN).

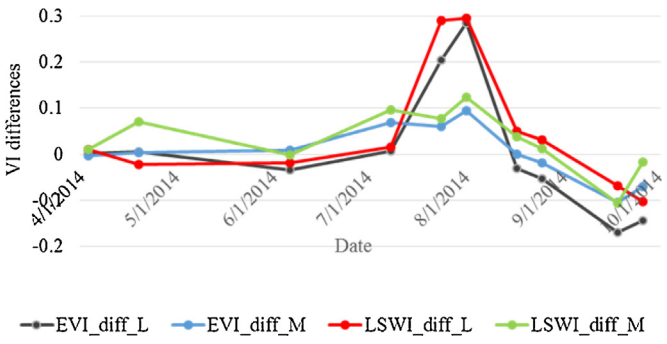

Fig. 8. Differences in Enhanced Vegetation Index (EVI) and Land Surface Water Index (LSWI) at iGOS WN and iGOS W MODIS pixel derived from MODIS and Landsat images.

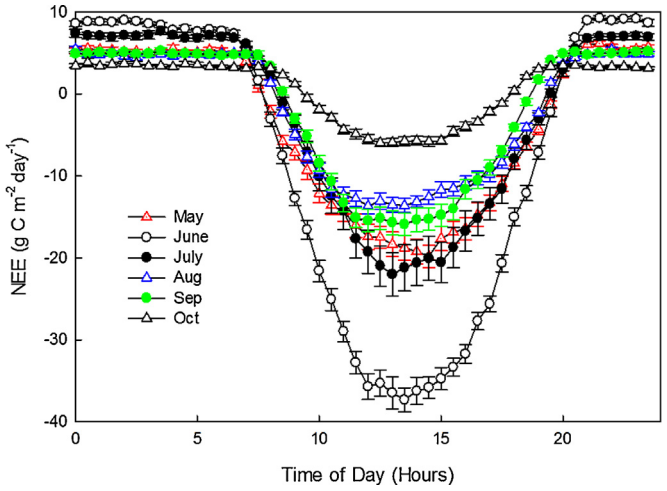

Fig. 9. Half-hourly binned diurnal courses of net ecosystem CO_2 exchange (NEE) from May to October 2014 at the iGOS W site. Negative values of NEE indicate net carbon uptake and positive values indicate carbon release by the ecosystem. Each data point is a mean value for the specific time step for the entire month and bars represent standard errors of the means.

differences in VIs between iGOS W and iGOS WN, most likely due to the similar grazing intensity.

3.1.4. Differences in VIs between iGOS WN and iGOS W derived from MODIS and landsat images

The EVI and LSWI differences between iGOS WN and iGOS W derived from MODIS images varied between −0.1 to 0.1 throughout the growing season (Fig. 8). The relatively larger differences in EVI and LSWI between two pixels derived from Landsat images were observed after the first baling (0.3) and during senescence (-0.1). The EVI differences derived from both MODIS and Landsat images showed that EVI in iGOS W was higher (by around 0.1) than iGOS WN at the beginning of October, which indicates re-growth of more photosynthetically active vegetation after baling.

3.2. Carbon fluxes in response to management practices as observed by eddy flux tower

Diurnal patterns of NEE in the pasture across the growing season in 2014 are presented in Fig. 9. As expected, NEE increased with the increasing photosynthetic capacity and NEE rates decreased during the late growing season because of senescence of plants. The magnitude of daily NEE reached up to $-11.51\ g\,C\,m^{-2}\ day^{-1}$. The iGOS W was a carbon sink (i.e., negative NEE values) for most of the growing season until late October when it turned to carbon neutral. Baling changed NEE values from negative to positive (from carbon sink to

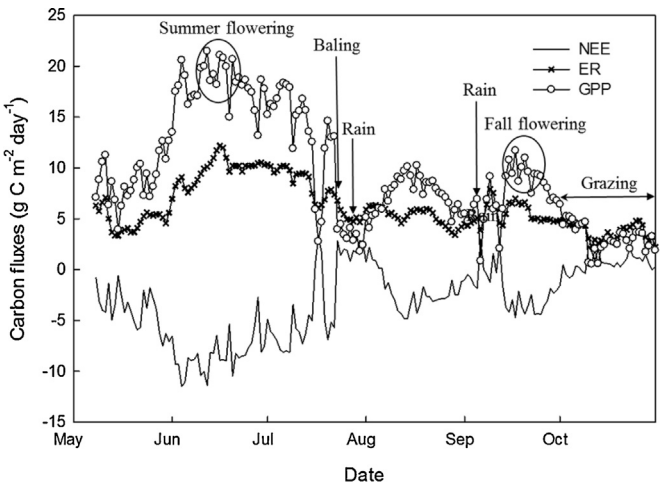

Fig. 10. Daily sums of gross primary production (GPP), ecosystem respiration (ER), and net ecosystem CO_2 exchange (NEE) from flux tower in the 2014 growing season.

carbon source). The magnitudes of diurnal peak NEE (monthly average) reached up to $-37.33 \pm 1.46\ \mu mol\ m^{-2}\ s^{-1}$ in June (leaf area index: 5.95 and aboveground biomass: $563.44\ g/m^2$) and declined quickly in July ($-22.02 \pm 2.68\ \mu mol\ m^{-2}\ s^{-1}$). The diurnal patterns of NEE in May and July were similar. It is noteworthy to mention that NEE in September was higher than in August, which showing that the pasture was a stronger carbon sink in September than in August.

The seasonal pattern of GPP was similar to NEE but with the opposite sign (Fig. 10). The magnitude of daily GPP reached up to $21.47\ g\,C\,m^{-2}\ day^{-1}$. ER had small variation during the growing season (approximately $5\ g\,C\,m^{-2}\ day^{-1}$) except for June and early July when it reached about $12\ g\,C\,m^{-2}\ day^{-1}$. A decreasing trend of GPP was observed after early June and dropped abruptly in mid-July because of cloudy (also indicated by very low PAR in Fig. 2) and windy weather (identified from PhenoCam images during this period). As expected, GPP decreased more than ER after baling, turning the grassland into a net carbon source for approximately 10 days. After that period, both GPP and NEE increased rapidly again which might have been triggered by re-growth of vegetation and two large rain events (~50 mm/day) at the end of July and early September (Fig. 2). These two peaks for GPP after baling had similar magnitudes ($\sim 10\ g\,C\,m^{-2}\ day^{-1}$). Grazing in the late growing season did not affect carbon dynamics substantially.

3.3. GPP in response to management practices and disturbance as estimated by VPM

3.3.1. GPP simulation from VPM

GPP_{EC} was highly correlated with EVI (Fig. 11a), showing the capability of EVI to track GPP. GPP_{VPM_W} captured the trends of GPP_{EC} very well ($r^2 = 0.89$) throughout the growing season (Fig. 11b). Three peaks of GPP_{EC} were also tracked by GPP_{VPM_W}. GPP_{EC} decreased sharply immediately after baling and it began to increase again with increasing greenness in the baled area, which as well captured by GPP_{VPM}. This result strengthens the comparison of GPP_{VPM} for baled and unbaled conditions. The VPM tended to underestimate GPP in the early stages of flowering (head emergence) which was detected from PhenoCam images (Fig. 3c and h). For example, GPP_{VPM} were smaller than GPP_{EC} values for mid-June and mid-September.

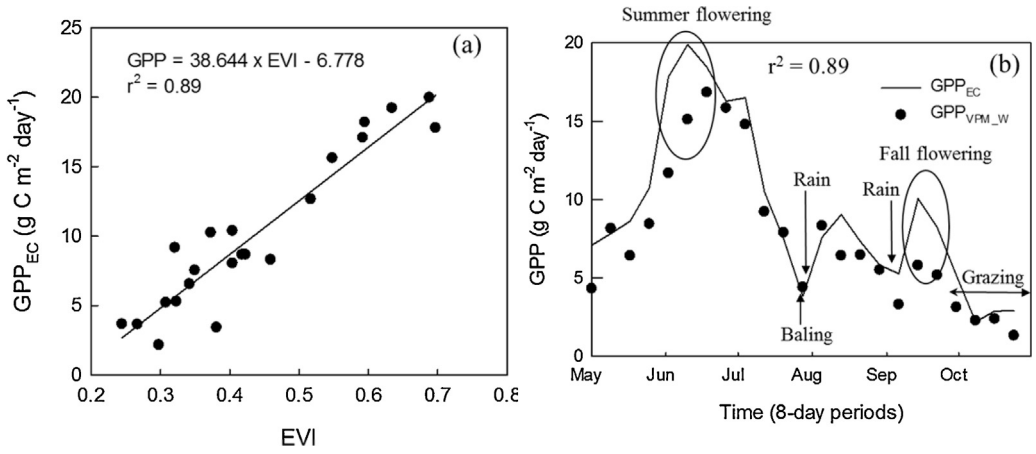

Fig. 11. (a) Relationship between enhanced vegetation index (EVI) and gross primary production (GPP_{EC}). (b) Comparison between gross primary production (GPP) from VPM simulation and EC measurement (GPP_{VPM_W} and GPP_{EC}).

Table 1
Event based GPP statistics for iGOS W and iGOS WN.

Event	Time point or period in 8-days	GPP_{VPM_W} ($g\,C\,m^{-2}\,day^{-1}$)	GPP_{VPM_WN} ($g\,C\,m^{-2}\,day^{-1}$)
1. Before field campaign	May 1st–June 2nd	7.799	7.790
2. Field campaign	Mid-June		
a. 2 weeks after field campaign	June 10th–July 18th	15.962	12.633
b. 3–5 weeks after field campaign	June 26th–July 12nd	13.278	13.629
Average	June 10th–July 12nd	14.352	13.230
3. The first baling	July 23rd		
a. 2 weeks after baling	July 20th–July 28th	6.143	8.157
b. 3–7 weeks after baling	Aug. 5th–Sept. 6th	6.004	5.758
c. 8–9 weeks after baling	Sept. 14th–Sept. 22nd	5.484	4.098
Average	July 20th–Sept. 22nd	5.920	5.922
4. Grazing	Sept. 30th–Oct. 24th	2.277	2.294
Whole growing season	May 1st–Oct. 24th	7.528	7.286

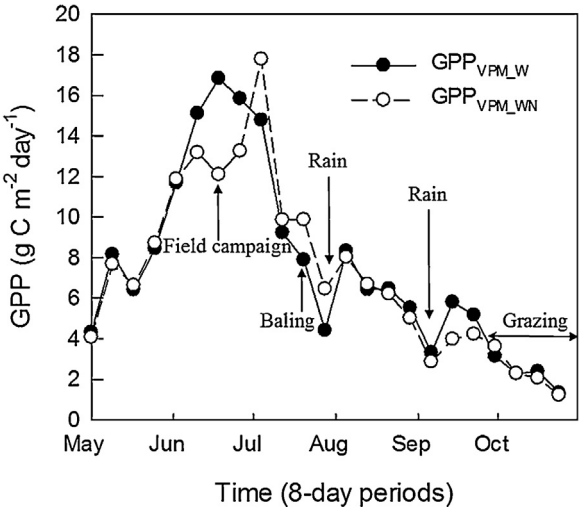

Fig. 12. Differences in gross primary production (GPP) difference of the flux tower located pixel (iGOSW) and its neighbor pixel (iGOS WN).

3.3.2. GPP in response to intensive field campaign, baling, and grazing as estimated by VPM

GPP_{VPM_W} and GPP_{VPM_WN} were very similar in May, August, and October (Fig. 12) because of little differences in VIs and the identical meteorological data input into the VPM. Event-based GPP statistics are presented in Table 1 to reflect impacts of intensive field research campaign, baling, and grazing. Before the intensive field research campaign in mid-June, GPP_{VPM_W} and GPP_{VPM_WN} were almost identical. The intensive field research campaign in iGOS WN caused the lower GPP values than in iGOS W (12.633 $g\,C\,m^{-2}\,day^{-1}$ vs. 15.962 $g\,C\,m^{-2}\,day^{-1}$). The GPP difference caused by the intensive field research campaign disappeared around mid-July as GPP_{VPM_W} and GPP_{VPM_WN} became similar (Fig. 12). Baling (July 23rd) decreased GPP_{VPM_W} by around 2 $g\,C\,m^{-2}\,day^{-1}$ for the following two 8-day periods. GPP_{VPM_W} and GPP_{VPM_WN} converged again in early August and remained similar for the rest of the month. Following the large rain events in late July and early September (Fig. 2) both GPP_{VPM_W} and GPP_{VPM_WN} increased, with GPP_{VPM_W} having a higher magnitude because of more photosynthetically active vegetation in iGOS W after baling. This compensated for the decreased GPP due to baling and resulted in negligible difference between GPP_{VPM_W} and GPP_{VPM_WN} (-0.002 $g\,C\,m^{-2}\,day^{-1}$) for the period after baling to before grazing (July 20th – September 22th). The late growing-season grazing in the whole field did not exert different impacts at iGOS W and iGOS WN. With different management practices, the growing season average GPP was similar (7.528 $g\,C\,m^{-2}\,day^{-1}$ in iGOS W and 7.286 $g\,C\,m^{-2}\,day^{-1}$ in iGOS WN).

4. Discussion

4.1. Necessity of utilizing multiple observations to study the impacts of management practices on plant phenology and carbon fluxes

This study incorporated PhenoCam images, satellite remote sensing products, and eddy covariance data to investigate the impacts of burning, baling, and grazing on vegetation phenology and GPP of a Old World bluestems pasture. Because of different spatial and temporal resolutions of data sources, their applications

on detecting the impacts of management practices are different. Since PhenoCam provide high temporal frequency *in situ* images, it is suitable for detecting plant phenology. Satellite remote sensing has larger spatial coverage than PhenoCam which makes it suitable for investigating larger scale events (e.g. characterizing the baling affected area). The EC data quantifies the impacts of management practices on carbon fluxes and provides data to evaluate GPP models. Combination of remote sensing and EC data in VPM for disturbed and undisturbed scenarios allowed assessment of the impacts of intensive field research campaign and baling on GPP. Multiple datasets allowed an investigation of intra-annual variations caused by different management practices.

PhenoCam has been a popular tool to study plant phenology (Migliavacca et al., 2011; Richardson et al., 2007; Richardson et al., 2013). PhenoCam images vividly showed the management practices (burning, baling, and grazing) and the quick recovery of grassland after baling (Fig. 3). The underestimation of GPP from VPM (Fig. 11b) was attributed to the underestimation of VIs for the early stages of flowering (seed heads tend to have lower VIs values than leaves because of lower chlorophyll content.), which was identified from PhenoCam images (Fig. 3c and h and Fig. 5). The *in situ* observation from PhenoCam indicated its potential applications in ecosystem management studies as an aided tool.

Satellite remote sensing provides observations at larger spatial scale than does PhenoCam but at lower temporal resolution. Free satellite remote sensing data, namely MODIS and Landsat, are suitable for different purposes depending on the temporal and spatial scales and objectives of the study. The 8-day temporal resolution of MODIS makes it well suited to quantify GPP dynamics, while the higher spatial resolution of Landsat (30 m) allows quantification of areas affected by various small-scale management practices (Fig. 6). Although the higher spatial resolution of Landsat image provides more detail at the land surface, the lower temporal resolution (16-day) limits its application in remote sensing based GPP models. Sixteen days between observations are long periods of time for characterizing vegetation, especially grasslands and crops. In addition, some observations are affected by cloud covers. Thus, Landsat may not be suitable to track the recovery trajectory of vegetation. For example, Landsat images were not available during the intensive field research campaign, while MODIS images captured this event well (Fig. 7). Thus, combining observations from Landsat and other high spatial resolution sensors (e.g., SPOT HRB/HRVIS and Sentinel-2A/B) can help to alleviate this issue.

With a single flux tower site, we simulated GPP using VPM for both disturbed and undisturbed scenarios. This approach of combining remote sensing and EC data to study the impacts of management practices on GPP helps to extend the use of EC data collected within flux networks (e.g., AmeriFlux and FLUXNET) to study the impacts of management practices (Campioli et al., 2015) in cases where paired-tower data are not available.

4.2. Complexity of assessing the impacts of management practices

There are a multitude of management practices that can occur in different durations and intensities. Most pastures in the Great Plains are used to support livestock grazing. The management practices evaluated in this study (burning, baling, and grazing) are quite common in the tallgrass pasture region (Fischer et al., 2012; Luo et al., 2009; Owensby et al., 2006; Suyker et al., 2003). The grassland greened up immediately after burning in April. Our results showed quick recovery (about one month) of grassland after baling. The pasture was a stronger carbon sink in September than in August mostly because of more precipitation in September. The net overall effect of baling on GPP was negligible because of the fact that baling enhanced the production in the post-baling period and resulted in higher GPP than the unbaled condition. The effect of baling may have been confounded by climatic conditions as well. For example, large rain events in late July and early September increased GPP, possibly offsetting the reduction in GPP caused by baling. Because of the large variability in climate from year to year, this may not be the case for baling in other years or locations. Beside climatic conditions, timing and intensity (e.g., stubble height) of baling could also play important roles in determining the response/recovery of ecosystem from the disturbances. To better understand the impacts of baling and other management activities, multiple years of data and consideration of interaction between management practices and climatic conditions (Fischer et al., 2012; Luo et al., 2012; Wagle et al., 2015) are needed. Grazing in the late growing season had similar impacts on VIs and GPP in both iGOS W and iGOS WN, indicating similar grazing intensity over the entire field. To investigate the impacts of grazing, comparison between grazed and un-grazed fields is needed.

4.3. Importance of the examination of EC footprint

As GPP_{EC} was used to evaluate the performance of VPM, we assume that the EC system and MODIS observed the same area. To test this assumption, we overlapped the EC footprint with the affected area characterized by Landsat images during different periods (Fig. 13). Contribution of flux measurements outside the iGOS W MODIS pixel boundaries can be detected by flux tower, while it cannot be detected using VIs derived from MODIS. The peak contribution of flux measurement from the upwind distance increased from 50 to 60 m before the first baling (Fig. 13a) to 80–90 m after the first baling (Fig. 13b and c). This discrepancy may be a function of decreased roughness due to reduced canopy height after baling (Chen et al., 2011; Chen et al., 2012; Schmid 1994). Since the flux tower is 100 m away from the southern boundary of the iGOS W pixel, the second baling in the southeastern part of the field had little effect on the flux measurement (Fig. 13c). This observation suggests that we need to bring the EC footprint dynamics (size, shape, and direction) into consideration because the affected areas in second baling might be in the fetch area and observed by the flux tower, while the iGOS W pixel cannot reflect this effect. If this scenario is the case then the pixel-to-pixel comparison in GPP model evaluation using EC measurements might be biased. Thus, investigating the dynamics of the footprint and its relative location to managed area is important to reflect the true impacts of management practices.

4.4. Implication and future steps

This comprehensive case study used different data sources to investigate the impacts of different management practices on grassland phenology and carbon dynamics. We quantified the impacts of disturbance from an intensive field research campaign and baling on GPP using a single flux tower data, satellite remote sensing data, and modeling. This approach could be used in other similar conditions for better utilization of carbon fluxes data to quantify the impacts of management practices. The study only includes one year of data. Thus, to better understand the interactive effects of management practices and climatic conditions, additional study years and sites are needed. There is a potential to use data from different networks (e.g., EC data from FLUXNET and PhenoCam images from PhenoCam Network) (Baldocchi et al., 2001; Richardson et al., 2009) to better understand impacts of various land management practices on plant phenology and carbon fluxes in different years.

The difference between GPP_{VPM_W} and GPP_{VPM_WN} was highly dependent on the differences in VIs for the two neighbor MODIS pixels. However, MODIS obscured this difference because of its spatial resolution. We showed large differences in the VIs derived from

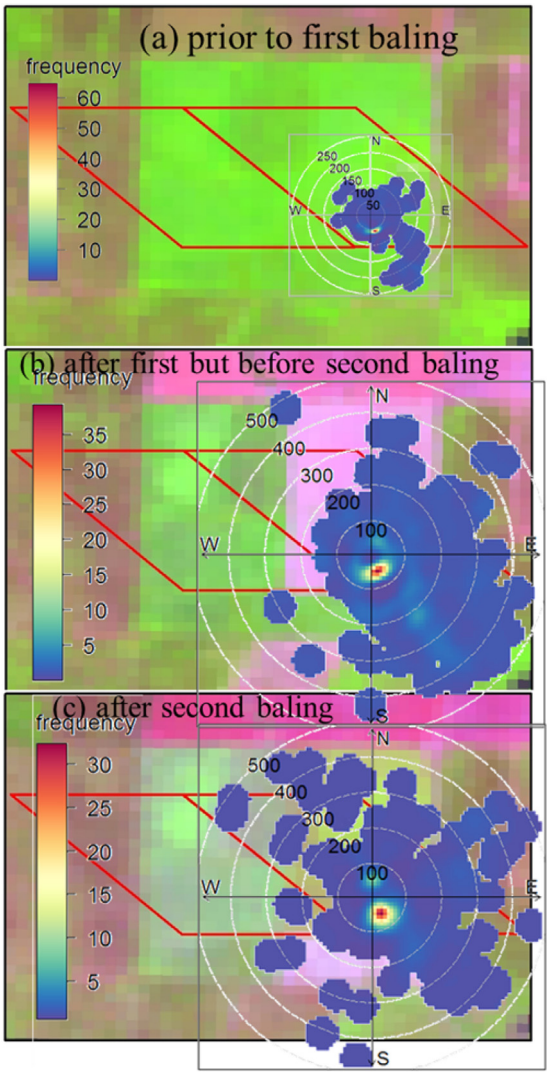

Fig. 13. Footprint before and after hay baling. (a) Prior to first baling, (b) after first but before second baling, (c) after second baling. The background images are from Landsat which showed conditions prior to baling, after the first baling, and after the second baling. The circular dots are contribution of flux measurements from different direction and distance. Colors indicate the frequency of contribution of flux measurements.

MODIS and Landsat images (Fig. 8), which needs further research. The low temporal resolution of Landsat also limited the ability to detect GPP dynamics over short periods of time.

Although we proposed a way to simulate the impacts of management practices and disturbances on GPP in a complex agricultural production field, additional research is needed to better estimate the individual and confounding effects of different management practices. Ensuring the fetch area of the flux tower can reduce the effects of changed footprint on GPP model and management evaluation (Chen et al., 2011; Chen et al., 2012). Locating the flux tower in the center of the MODIS pixel can facilitate the linkage between EC and satellite observations (Zhang et al., 2014). Each management regime needs better understanding before we blend different management practices. The compounding effects of interactive management practices need further examination with multiyear data. For example, burning in the early growing season might increase nutrient availability and affect the response of the field to baling.

5. Conclusion

This case study used digital repeat photography (PhenoCam), satellite remote sensing, and the eddy covariance technique to investigate the impacts of burning, baling, and grazing on plant phenology and carbon fluxes in a Old World bluestems pasture. Multiple datasets allowed studying intra-annual variations caused by various management practices. PhenoCam images provided valuable information for both management practices and plant phenology. MODIS and Landsat images reflected different aspects of management practices. Higher temporal resolution of MODIS helped in understanding the GPP dynamics, whereas Landsat detected the burning and baling affected area because of its higher spatial resolution. VIs from MODIS showed impacts of burning and baling on plant phenology. Responses of GPP in baled and unbaled grasslands to large rain events were different because of different stages of vegetation. The larger increase of GPP after large rain in baled grassland (photosynthetically more active vegetation) compensated the reduction in GPP caused by baling. This result indicated that the interaction of management practices with climate is important when studying their impacts on GPP. Since management practices are often complex (e.g, grazing and baling in pasture), we need multiyear data from different sources for better understanding of individual and confounding impacts of those management practices. Investigation of the dynamics of EC footprint and its relative geolocation to affected area is important when evaluating the impacts of management practices. The approach of integrating EC data with remote sensing to study the impacts of management practices on plant phenology and carbon fluxes can be helpful to extend the usage of EC data collected within the flux networks (e.g., AmeriFlux and FLUXNET) to study the impacts of different management practices.

Acknowledgements

This study was supported in part by research grants from the USDA National Institute of Food and Agriculture (grant number 2013-69002-23146 and 2016-68002-24967), the National Science Foundation (NSF)EPSCoR (grant number IIA-1301789), and NOAA Climate Office's Sectoral Applications Research Program (SRP) grant NA130AR431012. We would like to acknowledge Dr. Ming Chen for his suggestions in the early stage of the manuscript and Russell B. Doughty for English editing of the manuscript.

References

Baldocchi, D., Falge, E., Gu, L., Olson, R., Hollinger, D., Running, S., Anthoni, P., Bernhofer, C., Davis, K., Evans, R., Fuentes, J., Goldstein, A., Katul, G., Law, B., Lee, X., Malhi, Y., Meyers, T., Munger, W., Oechel, W., Paw, K.T., Pilegaard, K., Schmid, H.P., Valentini, R., Verma, S., Vesala, T., Wilson, K., Wofsy, S., 2001. FLUXNET: a new tool to study the temporal and spatial variability of ecosystem–scale carbon dioxide, water vapor, and energy flux densities. Bull. Am. Meteorol. Soc. 82, 2415–2434.

Brockway, D.G., Gatewood, R.G., Paris, R.B., 2002. Restoring fire as an ecological process in shortgrass prairie ecosystems: initial effects of prescribed burning during the dormant and growing seasons. J. Environ. Manage. 65, 135–152.

Campioli, M., Vicca, S., Luyssaert, S., Bilcke, J., Ceschia, E., Chapin III, F., Ciais, P., Fernández-Martínez, M., Malhi, Y., Obersteiner, M., 2015. Biomass production efficiency controlled by management in temperate and boreal ecosystems. Nat. Geosci. 8, 843–846.

Chen, B., Coops, N.C., Fu, D., Margolis, H.A., Amiro, B.D., Barr, A.G., Black, T.A., Arain, M.A., Bourque, C.P.-A., Flanagan, L.B., 2011. Assessing eddy-covariance flux tower location bias across the Fluxnet-Canada Research Network based on remote sensing and footprint modelling. Agric. Forest Meteorol. 151, 87–100.

Chen, B., Coops, N.C., Fu, D., Margolis, H.A., Amiro, B.D., Black, T.A., Arain, M.A., Barr, A.G., Bourque, C.P.-A., Flanagan, L.B., 2012. Characterizing spatial representativeness of flux tower eddy-covariance measurements across the Canadian Carbon Program Network using remote sensing and footprint analysis. Remote Sens. Environ. 124, 742–755.

Chi, J., Waldo, S., Pressley, S., O'Keeffe, P., Huggins, D., Stöckle, C., Pan, W.L., Brooks, E., Lamb, B., 2016. Assessing carbon and water dynamics of no-till and

conventional tillage cropping systems in the inland Pacific Northwest US using the eddy covariance method. Agric. Forest Meteorol. 218, 37–49.
Dong, J.W., Xiao, X.M., Wagle, P., Zhang, G.L., Zhou, Y.T., Jin, C., Torn, M.S., Meyers, T.P., Suyker, A.E., Wang, J.B., Yan, H.M., Biradar, C., Moore, B., 2015. Comparison of four EVI-based models for estimating gross primary production of maize and soybean croplands and tallgrass prairie under severe drought. Remote Sens. Environ. 162, 154–168.
Falge, E., Baldocchi, D., Olson, R., Anthoni, P., Aubinet, M., Bernhofer, C., Burba, G., Ceulemans, R., Clement, R., Dolman, H., 2001. Gap filling strategies for defensible annual sums of net ecosystem exchange. Agric. Forest Meteorol. 107, 43–69.
Fischer, M.L., Torn, M.S., Billesbach, D.P., Doyle, G., Northup, B., Biraud, S.C., 2012. Carbon, water: and heat flux responses to experimental burning and drought in a tallgrass prairie. Agric. Forest Meteorol. 166, 169–174.
Jin, C., Xiao, X., Merbold, L., Arneth, A., Veenendaal, E., Kutsch, W.L., 2013. Phenology and gross primary production of two dominant savanna woodland ecosystems in Southern Africa. Remote Sens. Environ. 135, 189–201.
Lloyd, J., Taylor, J., 1994. On the temperature dependence of soil respiration. Funct. Ecol., 315–323.
Luo, Y., Sherry, R., Zhou, X., Wan, S., 2009. Terrestrial carbon-cycle feedback to climate warming: experimental evidence on plant regulation and impacts of biofuel feedstock harvest. GCB Bioenergy 1, 62–74.
Luo, G., Han, Q., Zhou, D., Li, L., Chen, X., Li, Y., Hu, Y., Li, B.L., 2012. Moderate grazing can promote aboveground primary production of grassland under water stress. Ecol. Complexity 11, 126–136.
McPherson, R.A., Fiebrich, C.A., Crawford, K.C., Kilby, J.R., Grimsley, D.L., Martinez, J.E., Basara, J.B., Illston, B.G., Morris, D.A., Kloesel, K.A., 2007. Statewide monitoring of the mesoscale environment: a technical update on the Oklahoma Mesonet. J. Atmos. Oceanic Technol. 24, 301–321.
Migliavacca, M., Galvagno, M., Cremonese, E., Rossini, M., Meroni, M., Sonnentag, O., Cogliati, S., Manca, G., Diotri, F., Busetto, L., Cescatti, A., Colombo, R., Fava, F., Morra di Cella, U., Pari, E., Siniscalco, C., Richardson, A.D., 2011. Using digital repeat photography and eddy covariance data to model grassland phenology and photosynthetic CO2 uptake. Agric. Forest Meteorol. 151, 1325–1337.
Moffat, A.M., Papale, D., Reichstein, M., Hollinger, D.Y., Richardson, A.D., Barr, A.G., Beckstein, C., Braswell, B.H., Churkina, G., Desai, A.R., Falge, E., Gove, J.H., Heimann, M., Hui, D., Jarvis, A.J., Kattge, J., Noormets, A., Stauch, V.J., 2007. Comprehensive comparison of gap-filling techniques for eddy covariance net carbon fluxes. Agric. Forest Meteorol. 147, 209–232.
Niu, S., Sherry, R.A., Zhou, X., Luo, Y., 2013. Ecosystem carbon fluxes in response to warming and clipping in a tallgrass prairie. Ecosystems 16, 948–961.
Owensby, C.E., Ham, J.M., Auen, L.M., 2006. Fluxes of CO 2 from grazed and ungrazed tallgrass prairie. Rangeland Ecol. Manage. 59, 111–127.
Potter, C.S., Randerson, J.T., Field, C.B., Matson, P.A., Vitousek, P.M., Mooney, H.A., Klooster, S.A., 1993. Terrestrial ecosystem production: a process model based on global satellite and surface data. Global Biogeochem. Cycles 7, 811–841.
Reichstein, M., Falge, E., Baldocchi, D., Papale, D., Aubinet, M., Berbigier, P., Bernhofer, C., Buchmann, N., Gilmanov, T., Granier, A., 2005. On the separation of net ecosystem exchange into assimilation and ecosystem respiration: review and improved algorithm. Global Change Biol. 11, 1424–1439.
Reinhart, K.O., Dangi, S.R., Vermeire, L.T., 2016. The effect of fire intensity, nutrients, soil microbes, and spatial distance on grassland productivity. Plant Soil, 1–14.
Richardson, A.D., Jenkins, J.P., Braswell, B.H., Hollinger, D.Y., Ollinger, S.V., Smith, M.-L., 2007. Use of digital webcam images to track spring green-up in a deciduous broadleaf forest. Oecologia 152, 323–334.
Richardson, A.D., Braswell, B.H., Hollinger, D.Y., Jenkins, J.P., Ollinger, S.V., 2009. Near-surface remote sensing of spatial and temporal variation in canopy phenology. Ecol. Appl. 19, 1417–1428.
Richardson, A.D., Keenan, T.F., Migliavacca, M., Ryu, Y., Sonnentag, O., Toomey, M., 2013. Climate change, phenology: and phenological control of vegetation feedbacks to the climate system. Agric. Forest Meteorol. 169, 156–173.
Rogiers, N., Eugster, W., Furger, M., Siegwolf, R., 2005. Effect of land management on ecosystem carbon fluxes at a subalpine grassland site in the Swiss Alps. Theor. Appl. Climatol. 80, 187–203.
Roy, D.P., Wulder, M., Loveland, T., Woodcock, C., Allen, R., Anderson, M., Helder, D., Irons, J., Johnson, D., Kennedy, R., 2014. Landsat-8: Science and product vision for terrestrial global change research. Remote Sens. Environ. 145, 154–172.
Running, S.W., Nemani, R.R., Heinsch, F.A., Zhao, M., Reeves, M., Hashimoto, H., 2004. A continuous satellite-derived measure of global terrestrial primary production. Bioscience 54, 547–560.
Samuel, W.C., Forbes, T.D.A., 1998. Herbage characteristics and performance of steers grazing old world bluestem. J. Range Manage. 51, 399–407.
Schmid, H.P., 1994. Source areas for scalars and scalar fluxes. Boundary Layer Meteorol. 67, 293–318.
Sims, D.A., Rahman, A.F., Cordova, V.D., El-Masri, B.Z., Baldocchi, D.D., Bolstad, P.V., Flanagan, L.B., Goldstein, A.H., Hollinger, D.Y., Misson, L., 2008. A new model of gross primary productivity for North American ecosystems based solely on the enhanced vegetation index and land surface temperature from MODIS. Remote Sens. Environ. 112, 1633–1646.
Staff, S.S., 1999. Soil Taxonomy: A Basic System of Soil Classification for Making and Interpreting Soil Surveys, 2nd edition. Natural Resources Conservation Service. U.S. Department of Agriculture Handbook 436.
teiner, J., 2014. Grazing CAP Newsletter, August, 2014. Available from: http://nebula.wsimg.com/30c933718adcb2a5e6347570dd69cfeb?AccessKeyId=989873E228CAF5DC44BB&disposition=0&alloworigin=1.
Suyker, A.E., Verma, S.B., Burba, G.G., 2003. Interannual variability in net CO2 exchange of a native tallgrass prairie. Global Change Biol. 9, 255–265.
Twidwell, D., Rogers, W.E., Fuhlendorf, S.D., Wonkka, C.L., Engle, D.M., Weir, J.R., Kreuter, U.P., Taylor, C.A., 2013. The rising Great Plains fire campaign: citizens' response to woody plant encroachment. Front. Ecol. Environ. 11, e64–e71.
Valkó, O., Török, P., Deák, B., Tóthmérész, B., 2014. Review: prospects and limitations of prescribed burning as a management tool in European grasslands. Basic Appl. Ecol. 15, 26–33.
Vermote, E., Vermeulen, A., 1999. Atmospheric correction algorithm: spectral reflectances (MOD09) ATBD version, 4.
Wagle, P., Kakani, V.G., 2014. Seasonal variability in net ecosystem carbon dioxide exchange over a young Switchgrass stand. GCB Bioenergy 6, 339–350.
Wagle, P., Xiao, X., Torn, M.S., Cook, D.R., Matamala, R., Fischer, M.L., Jin, C., Dong, J., Biradar, C., 2014. Sensitivity of vegetation indices and gross primary production of tallgrass prairie to severe drought. Remote Sens. Environ. 152, 1–14.
Wagle, P., Xiao, X., Suyker, A.E.1, 2015. Estimation and analysis of gross primary production of soybean under various management practices and drought conditions. ISPRS J. Photogramm. Remote Sens. 99, 70–83.
Wilson, D.M., Dalluge, D.L., Rover, M., Heaton, E.A., Brown, R.C., 2013. Crop management impacts biofuel quality: influence of switchgrass harvest time on yield, nitrogen and ash of fast pyrolysis products. Bioenergy Res. 6, 103–113.
Wu, C., Niu, Z., Gao, S., 2010. Gross primary production estimation from MODIS data with vegetation index and photosynthetically active radiation in maize. J. Geophys. Res.: Atmos. 115.
Xiao, X.M., Hollinger, D., Aber, J., Goltz, M., Davidson, E.A., Zhang, Q.Y., Moore, B., 2004a. Satellite-based modeling of gross primary production in an evergreen needleleaf forest. Remote Sens. Environ. 89, 519–534.
Xiao, X.M., Zhang, Q.Y., Braswell, B., Urbanski, S., Boles, S., Wofsy, S., Berrien, M., Ojima, D., 2004b. Modeling gross primary production of temperate deciduous broadleaf forest using satellite images and climate data. Remote Sens. Environ. 91, 256–270.
Yuan, W., Liu, S., Zhou, G., Zhou, G., Tieszen, L.L., Baldocchi, D., Bernhofer, C., Gholz, H., Goldstein, A.H., Goulden, M.L., 2007. Deriving a light use efficiency model from eddy covariance flux data for predicting daily gross primary production across biomes. Agric. Forest Meteorol. 143, 189–207.
Zeeman, M.J., Hiller, R., Gilgen, A.K., Michna, P., Plüss, P., Buchmann, N., Eugster, W., 2010. Management and climate impacts on net CO2 fluxes and carbon budgets of three grasslands along an elevational gradient in Switzerland. Agric. Forest Meteorol. 150, 519–530.
Zhang, X., Friedl, M.A., Schaaf, C.B., Strahler, A.H., Hodges, J.C., Gao, F., Reed, B.C., Huete, A., 2003. Monitoring vegetation phenology using MODIS. Remote Sens. Environ. 84, 471–475.
Zhang, Q., Cheng, Y.-B., Lyapustin, A.I., Wang, Y., Xiao, X., Suyker, A., Verma, S., Tan, B., Middleton, E.M., 2014. Estimation of crop gross primary production (GPP): I: impact of MODIS observation footprint and impact of vegetation BRDF characteristics. Agric. Forest Meteorol. 191, 51–63.
Zhou, Y., Xiao, X., Qin, Y., Dong, J., Zhang, G., Kou, W., Jin, C., Wang, J., Li, X., 2016. Mapping paddy rice planting area in rice-wetland coexistent areas through analysis of Landsat 8 OLI and MODIS images. Int. J. Appl. Earth Obs. Geoinf. 46, 1–12.